Journal of Power Sources 196 (2011) 2513–2518

Contents lists available at ScienceDirect

Journal of Power Sources

journal homepage: www.elsevier.com/locate/jpowsour

Study of a proton exchange membrane fuel cells catalyst subjected to anodic operating conditions, by synchrotron-based scanning photoelectron microscopy (SPEM) and high lateral-resolution X-ray photoelectron spectroscopy

Benedetto Bozzini [a,*], Matteo Amati [b], Marco Boniardi [c], Majid Kazemian Abyaneh [b], Luca Gregoratti [b], Maya Kiskinova [b]

[a] Dipartimento di Ingegneria dell'Innovazione, Università del Salento, via Monteroni s.n., 73100 Lecce, Italy
[b] Sincrotrone Trieste S.C.p.A., ELETTRA, s.s. 14 km 163.5 in Area Science Park, 34012 Basovizza, Trieste, Italy
[c] Dipartimento di Meccanica, Politecnico di Milano, via La Masa 34, 20156 Milano, Italy

ARTICLE INFO

Article history:
Received 12 August 2010
Received in revised form 29 October 2010
Accepted 7 November 2010
Available online 12 November 2010

Keywords:
SPEM
XPS
Electrocatalyst
Degradation
MEA

ABSTRACT

In this paper we report an investigation of the degradation of the Pt/C electrocatalyst of an anodic membrane-electrode assembly (MEA) after 1000 h of operation in a laboratory single-cell PEMFC, using synchrotron-based space-resolved photoelectron spectroscopy. This study is complemented by the analysis of a pristine MEA and reference materials, as well as by electrochemical measurements, SEM imaging and energy-dispersive X-ray fluorescence spectroscopy (EDX). Catalyst ageing correlates with a corrugation of morphology, as observed by SEM and scanning photoelectron microscopy (SPEM), corresponding to Pt nanoparticle agglomeration. Moreover – on the basis of high lateral resolution SPEM, X-ray photoelectron spectroscopy (XPS) and EDX analyses, – we found that, after operation, Pt is transported onto the fibres of the gas-diffusion layer (GDL). Space-resolved XPS shows a peak shift of the Pt $4f_{7/2}$ level to higher and lower binding energies with respect to Pt(1 1 1) and pristine Pt black, respectively, corresponding to nanocrystallinity in the first case and agglomeration in the second one. No oxidised Pt was found in any location of the anodically used MEA.

1. Introduction

One of the most critical barriers to the widespread commercial application of proton exchange membrane fuel cells (PEMFCs) is their durability, crucially impaired by catalyst stability. In fact, not only the well-known CO-poisoning problems impact the reliability of these systems, but also: (i) Pt dissolution from the cathode and recrystallisation in the PEM [1–3]; (ii) nanoparticle (NP) degradation, agglomeration and Pt surface-transport [4–10] and (iii) carbon-support corrosion and poisoning by corrosion products released by structural materials [11–15] affect the operation of fuel cells (FC) of both laboratory and commercial scales. In fact, Pt and Pt-alloy NPs, typically dispersed on high surface-area carbon black substrates, are extensively used as cathodic and anodic catalysts. The performance of catalysts degrades via complex – so far poorly understood – pathways, including: reduction of active surface due to agglomeration, clustering and sintering on one side and dissolution of Pt and corrosion of the carbon black on the other one.

The parameters empirically known to affect the morphological stability of Pt-based NP electrocatalysts – and consequently their efficiency – include: adsorption of oxidation intermediates, electrochemical polarisation and operating time. The topography of real solid surfaces plays an important role in defining the electronic energy distribution at surface sites, particularly when irregularities at the atomic level are taken into account. Likewise, surface irregularities at the nanometric level determine the electrocatalytic properties. In fact, the reactivity of small metal clusters has been found to vary by orders of magnitude when the cluster size is changed by only a few atoms [16] or monoatomic metallic layers are adsorbed onto the surfaces of NPs [17].

In the literature, frequent use is made of X-ray photoelectron spectroscopy (XPS) in order to characterise electrocatalysts, typically in the as-fabricated conditions. Nevertheless, the number of investigations on Pt/C-based materials after prolonged electrochemical polarisation is rather limited (see below for further details). Moreover, use of space-dependent XPS and photoelectron imaging is completely absent, to the best of the authors' knowledge. Wang et al. [15] report XPS measurements of Pt/C electrocatalysts before and after 10,000 potential cycles between 0.6 and 1.2 V_{RHE}: an increase of the relative amount of Pt(0) to Pt(II) has been found, interpreted in terms of Pt dissolution and redeposition, result-

* Corresponding author. Tel.: +39 0832 297323; fax: +39 0832 297111.
E-mail address: benedetto.bozzini@unile.it (B. Bozzini).

0378-7753/$ – see front matter © 2010 Elsevier B.V. All rights reserved.
doi:10.1016/j.jpowsour.2010.11.039

ing in Ostwald's ripening. Shao et al. [8] investigated by XPS the effects of repeated application of potential steps (from 0.60 or 0.85 to 1.4 V_{RHE}) and prolonged potentiostatic polarisation (at 1.2 and 1.4 V_{RHE}) on the degradation of Pt/C:O and C were found to increase and the C peak has been shown to shift towards the formation of oxidised C species. Similar conclusions have been reached in [18] that applied 800 potentiodynamic cycles between 0 and 1.5 V_{RHE}.

XPS work on real membrane-electrode assemblies (MEAs) has been reported in [19,20]. The former investigation – involving a commercial MEA and one fabricated by the authors – was based on potential cycling in an aqueous solution and concentrated on quantitative elemental analysis in view of performance optimisation. The latter paper reports on the degradation of a Pt–Ru catalyst implemented in a MEA, caused by cell reversal during starvation. Quantitative elemental analysis carried out by XPS measurements of a fragment from the MEA disclosed changes in C and O content and, in particular, highlighted the decrease of Pt content in the catalyst alloy.

In the present investigation, we mean to address the point of the space-dependent chemical state of Pt, through synchrotron-based X-ray spectromicroscopy approaches: scanning photoelectron microscopy (SPEM) and XPS with nanometric lateral resolution. In this work, we compare catalyst materials in their pristine state and after 1000 h of anodic operation in a simple laboratory scale single-cell PEMFC. Our choice of focussing on the anodic side of the MEA is dictated by the fact that this system – facing far less critical operating conditions than the cathodic side – has received less attention in terms of materials degradation. Notwithstanding the fact that anodic operation results in a lower damage rate, still important degradation phenomena are observed and, in particular, new kinds of phenomenology are found, worth addressing and rationalising in view of material optimisation. This kind of relatively fundamental investigation is expected to have a bearing on the synthesis and management of nanocrystalline electrocatalyst materials, since an insightful understanding of these stability issues is strongly required for the design of fuel-cell MEAs as well as MEA-GDL assemblies for applications in real-scale systems.

2. Materials and methods

In this research, we have concentrated on the anodic side of the MEA of a single-cell laboratory PEMFC with electrochemically active dimensions 5 cm × 5 cm, purchased from Materials Mates Italia S.r.l. (Milano). The commercial C-supported Pt catalyst exhibited the following properties: dimensions of Pt nanoparticles: ca. 6 nm, Pt loading: 1 mg cm^{-2}, composition of catalyst layer: 70 wt.% Pt/C, 30 wt.% PTFE. This catalyst was applied to the Nafion sheet, pretreated as described in [21]. The gas diffusion layers (GDLs) were carbon paper containing TiO_2 as stiffener. The end-plates were fabricated by punching AISI 304 foils of thickness 0.2 mm. The cell was run for a 1000 h run: operating details of this very experiment have been published in [22], where bipolar plate corrosion was studied. For reference purposes, we have considered the following materials: (i) Pt(1 1 1) disk (diameter: 10 mm, thickness 2 mm, roughness <30 nm, orientation accuracy better than 0.1°) from Mateck and (ii) Pt-black (Aldrich 205915).

The scanning electron microscopy (SEM) images and energy dispersive X-ray fluorescence spectroscopy (EDX) data of the samples have been recorded using a Jeol JSM 6480-LV microscope equipped with a SphinX 130 IXRF Systems energy dispersive X-ray spectrometer.

Compositional mapping and high lateral-resolution XPS measurements were carried out by using the scanning photoelectron microscope (SPEM) at the ESCA microscopy beamline at the ELETTRA synchrotron radiation facility located in Trieste, Italy where a synchrotron source X-ray beam is focused on the sample into a spot with a diameter of around 150 nm using Fresnel zone plate optics. In SPEM the sample can be raster scanned with respect to the microprobe. The microscope operates in imaging and spectroscopic modes. The imaging mode maps the lateral distribution of elements by collecting photoelectrons with a selected kinetic energy window while scanning the specimen with respect to the microprobe. When the element under consideration is present in a single chemical state, the spatial variation in the contrast of the images reflects the variation of the photoelectron yield, which is a measure of the local concentration of the element. The microspot mode is identical to the conventional XPS. Spatially resolved photoemission spectra of selected regions and chemical maps were acquired with 200 meV energy resolution by using 670 eV photon energy. More details on this microscope and on the beamline are provided in [23]. Before SPEM and XPS measurements, the Pt(1 1 1) single-crystal has been subjected to a sequence of sputtering and annealing processes, until a perfect low energy electron diffraction (LEED) pattern has been found. All the other samples were subjected to a light Ar-ion sputtering and checked for surface cleanliness by Auger electron spectroscopy (AES).

3. Results and discussion

3.1. SEM and EDX of the MEA in pristine and used conditions

After operation in the above-described conditions, the PEMFC was opened in view of analysing the catalyst layer of the MEA. It proved impossible to separate the MEA from the GDL without breaking off some fragments of the latter that were strongly sticking to the MEA itself. The exposed surface of the samples we

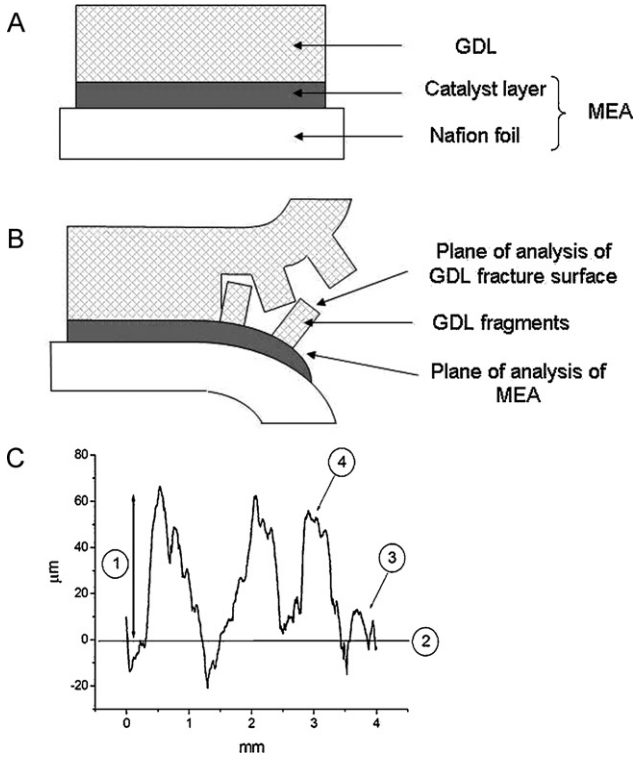

Fig. 1. Description of the analysed sample. (A) Schematic layout of the anodic MEA and GDL in pristine conditions. (B) Same, after operation and separation of MEA and GDL, leaving behind some GDL fragments, adhering to the MEA. (C) Typical Talystep line profile showing the dimensions of the GDL fragments and the locations of the analysed areas: (1) typical thickness of the GDL fragments, (2) nominal MEA/GDL interface, (3) plane of analysis of MEA, and (4) plane of analysis of GDL fracture surface.

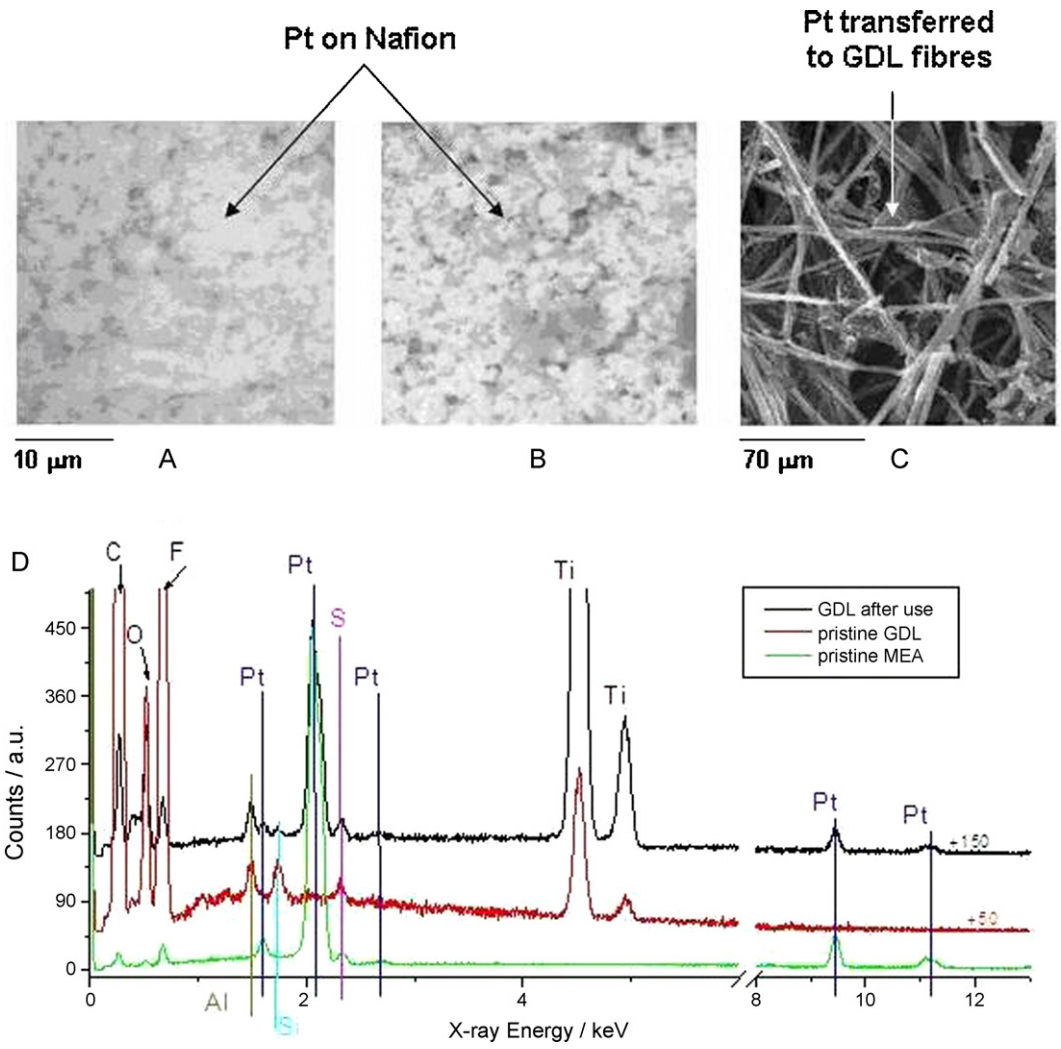

Fig. 2. SEM micrographs of: (A) catalyst layer of the MEA in pristine conditions; (B) same, used anodically for 1000 h (same magnification as (A)); (C) zone of the GDL adjacent to the anodically used catalyst layer; (D) EDX spectra measured in the area imaged in micrograph (C) as well as from pristine MEA and GDL.

analysed by SEM, EDX and SPEM therefore comprised both the MEA and fracture surfaces of the GDL, located about 0.1 mm above the actual MEA/GDL interface: Fig. 1 shows a schematic view of a typical sample as well as a representative Talystep profilometer trace, showing the accessible MEA and GDL planes of the sample. Fig. 2 shows SEM micrographs of the MEA surface in (A) pristine and (B) used conditions (1000 h, the region analysed corresponds to areas denominated "plane of analysis of MEA", location #3, in Fig. 1(C)). The fracture surface of the GDL fragments detected upon separating the used MEA denominated "plane of analysis of GDL fracture surface", location #4, in Fig. 1(C) is also shown in Fig. 2(C). After use in the PEMFC, the catalyst layer exhibits a more coarse-grained morphology that can be related to agglomeration of the Pt particles. Furthermore – after PEMFC operation – some Pt is transferred from the functionalised membrane to the GDL fibres, as proved by SPEM (see Section 3.2) and EDX (Fig. 2(D)) spectra measured on the area corresponding to the SEM image (Fig. 2(C)), disclosing the presence of the following elements: Pt from the catalyst, C from the catalyst support and from the GDL material and possibly from Nafion, F and S from Nafion and Ti from TiO_2, used as GDL filler; traces of Al and Si also result from the fabrication process. For comparison, EDX spectra on the MEA and GDL in pristine conditions are also reported in Fig. 2(D)). Of course, mainly Pt, with traces of F, S and C are found on the pristine MEA and just C and Ti, with traces of Al and Si, on the pristine GDL.

3.2. SPEM after operation in the PEMFC

In order to acquire reference spectra and to assess typical Pt distribution topologies, we performed SPEM measurements on the reference samples that are not extensively reported in this paper, for the sake of brevity. No measurable topology was found on the sputtered and annealed Pt(1 1 1) surface; Pt-black exhibits a granular topology, with typical dimensions of the order of 10–20 μm, corresponding to aggregates of submicrometric particles; the Pt/C ratio image shows micrometric aggregates of Pt NPs and a clear compositional contrast.

As far as the MEA after operation in the PEMFC is concerned, as reported in Section 3.1, Pt is found both in the original location on the functionalised Nafion membrane and on the GDL fibres contacting the membrane. We investigated by SPEM areas corresponding to the SEM micrographs shown in Fig. 2 (B: surface of the used functionalised membrane) and (C: GDL fibres in contact with the membrane). Our results are shown in Fig. 3: unused MEA, used-MEA and GDL, respectively. Pt transport from the MEA to the GDL has not been reported, to the best of the authors' knowledge, while a cognate phenomenon has been described: the recrystallisation of Pt in the bulk of the PEM, resulting from previous Pt dissolution [2,3]. These authors explain Pt displacement to the bulk of the Nafion foil by the reduction of Pt^{2+} by crossover hydrogen. Kim et al. [1] found that Pt, dissolved on the cathodic side of the MEA,

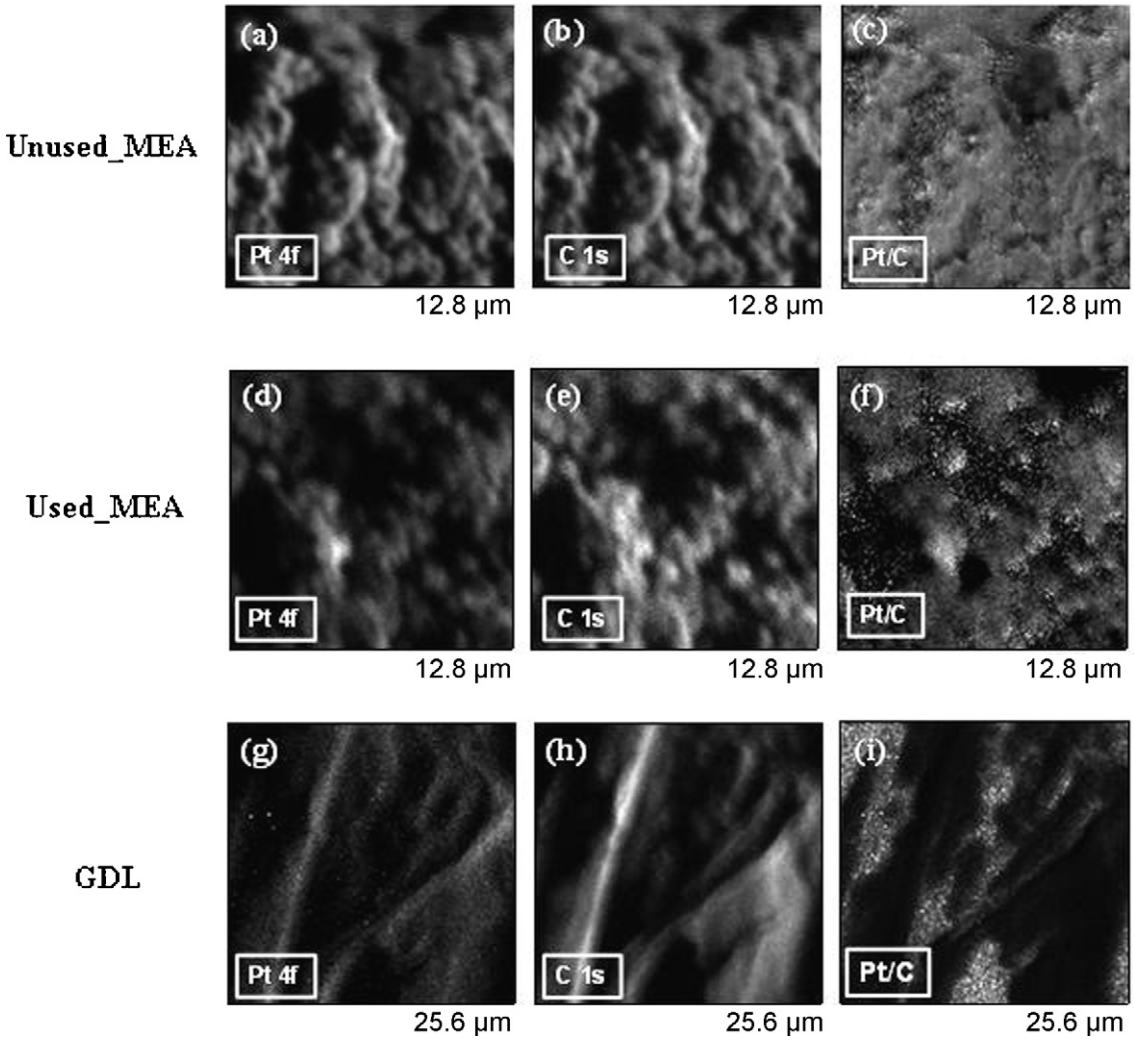

Fig. 3. Unused-MEA – SPEM images of the functionalised Nafion membrane in pristine conditions. Image (a) was recorded with photoelectrons energies set to 72 eV (Pt 4f), (b) was mapped with 284 eV (C 1s), (c) shows ratio of the Pt over (c) from images (a) and (b). Used-MEA – SPEM images of the functionalised Nafion membrane used anodically for 1000 h. Image (d) was recorded with photoelectron energies set to 72 eV (Pt 4f), (e) was mapped with 284 eV (C 1s) and (f) shows ratio of the Pt over C from images (d) and (e) GDL – SPEM images of a region of the GDL adjoining the anodic functionalised Nafion membrane after 1000 h of PEMFC operation. Images (g) and (h) were recorded with photon energies set to 72 (Pt 4f) and 284 (C 1s) eV, respectively. (i) Ratio of the Pt over C from images (g) and (h).

crossed the PEM and ended up reduced by hydrogen on the anodic side of the MEA. The formation of Pt^{2+} from active Pt nanoparticles of the anode catalyst can be expected [24]; furthermore, the action of anodically generated H_2O_2 resulting from O_2 crossover is liable to oxidise Pt [25–29]. Pt cations, most likely Pt^{2+}, can be easily transported in the GDL bulk where they can undergo reduction by hydrogen, according to the mechanism proposed in [1–3] for the bulk of the Nafion foil and a fortiori expected to be operative in the anodic GDL. From Fig. 3(a, b, d, and e) it can be noticed that the surface of the used functionalised membrane, showing a typical micrometric aggregate composed of submicrometric grains, exhibits a topology conforming to that found by SEM (see Fig. 2(B)), which is also similar to that found in the pristine conditions. The SPEM images obtained by monitoring the Pt 4f and C 1s core level emissions and the contrast variations convey both morphological and compositional information. Specifically, the brighter and darker areas can result from: (i) topography-related enhancement, (ii) shadowing of the electron emission or (iii) regions exhibiting different chemical compositions. The similar contrast visible in the pictures acquired at different elemental energies confirms that this is dominated by topographic artefacts rather than chemical heterogeneity. Nevertheless, slight changes in the chemical composition of the surfaces are highlighted in the Pt/C ratio images (Fig. 3(c)–(f)), where the presence of small bright areas discloses Pt agglomeration irrespective of the morphological and artefact contrast. Debris detached from the GDL, containing Pt localised on C fibres (see also Fig. 2(C) and (D)) can be imaged by SPEM. Fig. 3(g) and (h) reports $25.6 \times 25.6\ \mu m^2$ Pt 4f and C 1s photoelectron images, respectively. Fig. 3(i) shows the ratio of Pt over C computed from the SPEM maps (g) and (h) and exhibits a notable compositional contrast, highlighting the locations were Pt tends to agglomerate, following the fibrous structure.

3.3. High lateral-resolution XPS

In this investigation, we have studied the above-mentioned materials by space-dependent XPS of the following core levels: Pt 4f, C 1s and O 1s as well as of the valence-band (VB) region.

A set of representative Pt 4f spectra is reported in Fig. 4. Both Pt-based electrocatalyst materials are characterised by a peak shift with respect to the position of clean Pt(1 1 1): $4f_{7/2}$ 71.0 eV. The peak is found at higher BE in the case of Pt-black (71.2 eV) and the used-MEA (71.1 eV). These shifts correspond to modifications of the electronic structure of metallic Pt, probably resulting from

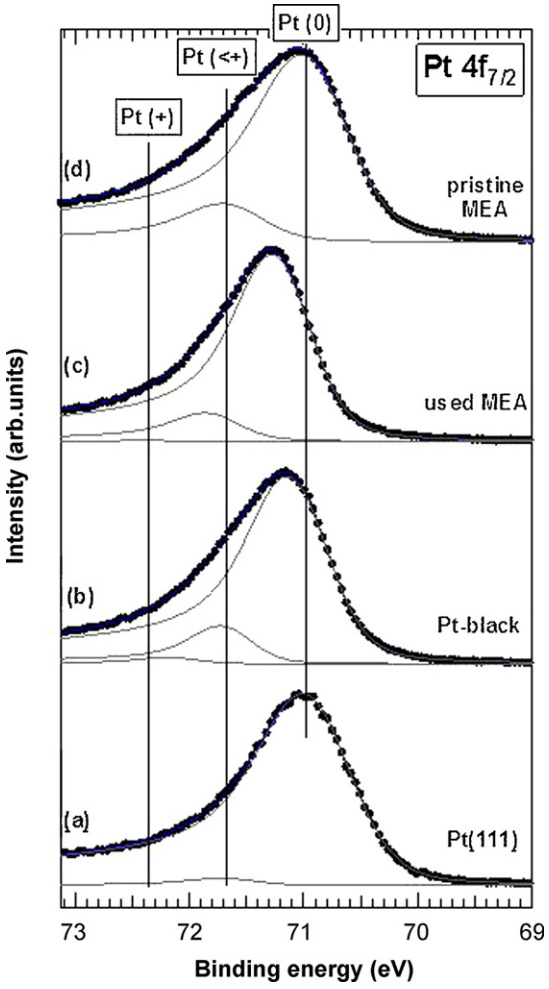

Fig. 4. High-resolution XPS Pt $4f_{7/2}$ spectra of the MEA in pristine conditions and used anodically for 1000 h, accompanied by reference spectra corresponding to Pt black and Pt(1 1 1).

nano crystallisation and agglomeration; the shifts are not enough to justify the formation of sizable amounts of Pt(II) and, a fortiori, of Pt(IV). It is worth noting that after prolonged (typically 800–10,000 cycles at 0.1 V s^{-1}) potentiodynamic cycling in the anodic range (up to 1.4 V RHE) the presence of Pt(II) has been found in E-TEK electrodes and that of Pt(IV) in Pt/C electrocatalysts deposited onto carbon cloth [19]. The asymmetric shape of the peaks at higher BEs has been resolved by a deconvolution procedure through the classical Doniach–Sunjich functions, disclosing the presence of small components at the $Pt^{(+)}$ and $Pt^{(<+)}$ energy positions. The area covered by these components does not exceed 20% of the total peak area. It is worth comparing these spectra with the Pt measured on the pristine MEA shown at the top of the figure. This spectrum appears much broader than the other ones and centred around 71.1 eV BE. The absence of oxygen in this material, as shown in Fig. 5(b), suggests that the broadening of the peak is mainly due to structural heterogeneity of the Pt nanoparticles supported on C.

VB spectra (not reported here for brevity) show that the threshold energy depends strongly on the particular type of system, but in all cases the typical shape found with clean Pt(1 1 1) is retained. The order of the shifts in energy – though not the amount of the shifts – mirrors that of the Pt 4f levels. According to [30], this can be interpreted with a predominant effect of the variation in the reference level among the different systems investigated, along with a minor contribution of charge-transfer (accounting for the changes in shift between the core level and the VB).

O 1s and C 1s spectra were also recorded in several locations of the pristine and used MEAs. Fig. 5 shows typical spectra compared with the same ones relative to the pristine material. No oxygen could be detected in the pristine MEA, while a well-defined peak is found with the used one. No essential changes in spectral shape were found for the O 1s peak as a function of location within the surface of the used MEA: the spectrum is centred at 532 eV BE. Such peak position is typical for oxidised C: values in this range have been found in the investigation of voltammetrically aged Pt/C on carbon cloth and E-TEK electrodes [19].

The XPS spectra of the C 1s level of the used-MEA exhibit a peak at 285.1 eV BE. Essentially the same peak position is found in every

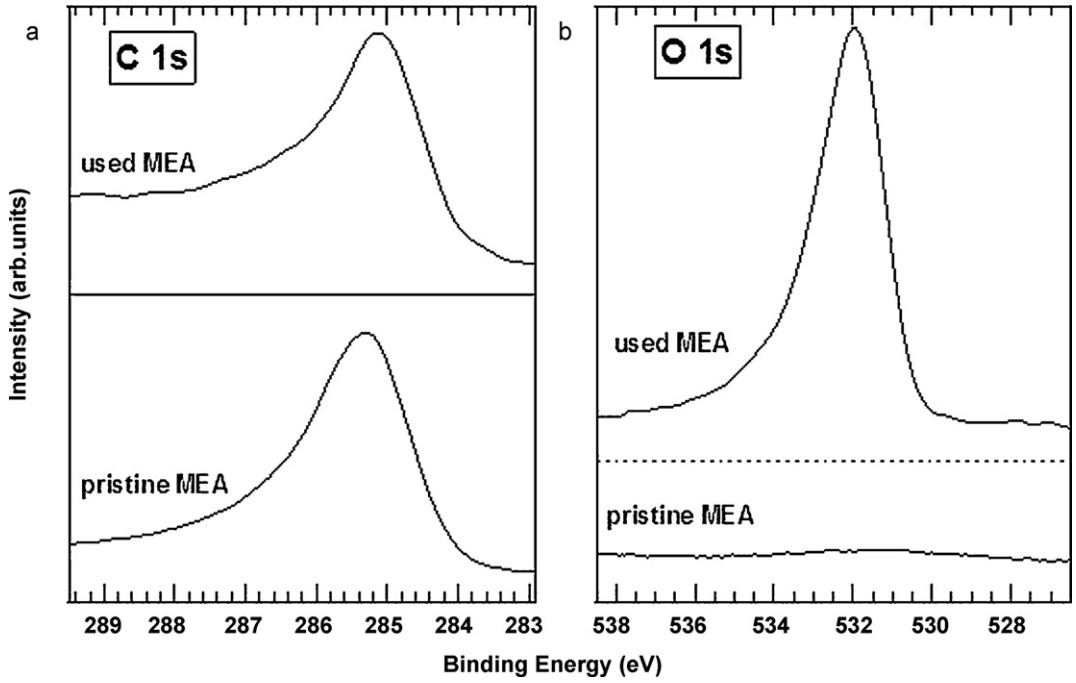

Fig. 5. High-resolution XPS C 1s and O 1s spectra of the MEA in pristine conditions and used anodically for 1000 h.

location. In the literature a wide range of C 1s BEs is reported, comprising both pristine (283.5/286.8 eV BE) and used (284.3/284.6) Pt/C electrocatalysts. A strict mechanistic assignment is therefore not possible, on the basis of literature data alone, nevertheless, a shift to higher BEs is compatible with C oxidation, which is a sensible scenario in our case.

4. Conclusions

In the present paper we have studied by SPEM and local XPS the chemical and morphological modifications – that can be traced by following the location and chemical state of Pt, C and O – of the Pt/C electrocatalyst of an anodic side of the MEA after 1000 h of operation in a laboratory PEMFC. Catalyst ageing was found to correlate with a corrugation of the Pt electrocatalyst in its original location, corresponding to Pt nanoparticle agglomeration. Furthermore, Pt has been found to be transported within the GDL, where it ends up fixed on the originally Pt-free C-paper fibres. Nanoparticle agglomeration could also be detected on the basis of shifts of the Pt $4f_{7/2}$ level. The anodic operation considered in this study has been found not to give rise to any kind of Pt oxidation. No O 1s signal is detected in the pristine MEA, while the peak measured in the used one is typical for oxidised C, as confirmed by the position of the C 1s peak.

References

[1] T. Kim, H. Lee, W. Sim, J. Lee, S. Kim, T. Lim, K. Park, Korean J. Chem. Eng. 26 (2009) 1265–1271.
[2] L. Franck-Lacaze, C. Bonnet, E. Choi, J. Moss, S. pomtvianne, H. Poirot, R. Datta, F. Lapicque, Int. J. Hydrogen Energy 35 (2010) 10472–10481.
[3] Ch.G. Chung, L. Kim, Y.W. Sung, J. Lee, J.S. Chung, Int. J. Hydrogen Energy 34 (2009) 8974–8981.
[4] F. Coloma, A. Sepulvedaescribano, J.L.G. Fierro, F. Rodriguez-Reinoso, Langmuir 10 (1994) 750–755.
[5] A. Guerrero-Ruiz, P. Badenes, I. Rodriguez-Ramos, Appl. Catal. A 173 (1998) 313–321.
[6] M. Kang, Y.S. Bae, C.H. Lee, Carbon 43 (2005) 1512–1516.
[7] M. Uchida, Y. Aoyama, M. Tanabe, N. Yanagihara, N. Eda, A. Ohta, J. Electrochem. Soc. 142 (1995) 2572–2576.
[8] Y. Shao, R. Kou, J. Wang, V.V. Viswanathan, J.H. Kwak, J. Liu, Y. Wang, Y. Lin, J. Power Sources 185 (2008) 280–286.
[9] M.S. Mamat, S.A. Grigoriev, K.A. Dzhus, D.M. Grant, G.S. Walker, Int. J. Hydrogen Energy 35 (2010) 7580–7587.
[10] A. Taniguchi, T. Akita, K. Yasuda, Y. Miyazaki, Int. J. Hydrogen Energy 33 (2008) 2323–2329.
[11] D.A. Stevens, J.R. Dahn, Carbon 43 (2005) 179–188.
[12] J.P. Meyers, R.M. Darling, J. Electrochem. Soc. 153 (2006) A1432–A1442.
[13] T. Yoda, H. Uchida, M. Watanabe, Electrochim. Acta 52 (2007) 5997–6005.
[14] C.H. Paik, G.S. Saloka, G.W. Graham, Electrochem. Solid-State Lett. 10 (2007) B39–B42.
[15] J. Wang, G. Yin, Y. Shao, Sh. Zhang, Zh. Wang, Y. Gao, J. Power Sources 171 (2007) 331–339.
[16] R.L. Whetten, D.M. Cox, D.J. Trevor, A. Kaldor, Phys. Rev. Lett. 54 (1985) 1494–1497.
[17] R.R. Adzic, J. Wang, B.M. Ocko, Electrochim. Acta 40 (1995) 83–89.
[18] J.M. Rheaume, B. Müller, M. Schulze, J. Power Sources 76 (1998) 60–68.
[19] W.R.W. Daud, A.B. Mohamad, A.A.H. Kadhum, R. Chebbi, S.E. Iyuke, Energy Conversion Manage. 45 (2004) 3239–3249.
[20] A. Taniguchi, T. Akita, K. Yasuda, Y. Miyazaki, J. Power Sources 130 (2004) 42–49.
[21] T.A. Zawodzinski, C. Derouin, S. Radzinski, R.J. Sherman, W.T. Smith, T.E. Springer, S. Gottesfeld, J. Electrochem. Soc. 140 (1993) 1041–1047.
[22] C. Mele, B. Bozzini, J. Power Sources 195 (2010) 3590–3596.
[23] L. Gregoratti, A. Barinov, E. Benfatto, G. Cautero, C. Fava, P. Lacovig, D. Lonza, M. Kiskinova, R. Tommasini, S. Mahl, Rev. Sci. Instrum. 75 (2004) 64–69.
[24] W. Bi, Th.F. Fuller, J. Power Sources 178 (2008) 188–196.
[25] E. Endoh, S. Terazono, W. Hardiyanto, Y. Takimoto, Electrochem. Solid State Lett. 7 (2004) A290.
[26] D.E. Curtin, R.D. Lousenberg, T.J. Henry, P.C. Tangeman, M.E. Tisack, J. Power Sources 131 (2004) 41–48.
[27] T. Kinumoto, M. Inaba, Y. Nakayama, K. Ogata, R. Umebayashi, A. Tasaka, Y. Iriyama, T. Abe, Z. Ogumi, J. Power Sources 158 (2006) 1222–1228.
[28] U.H. Jung, S.U. Jeong, K. Chun, K.T. park, H.M. Lee, D.W. Choi, S.H. Kim, J. Power Sources 170 (2007) 281–285.
[29] V.A. Sethuraman, J.W. Weidner, A.T. Haug, S. Motupally, L.V. Protsailo, J. Electrochem. Soc. 155 (2008) B50–B57.
[30] B.I. Boyanov, T.I. Morrison, J. Phys. Chem. 100 (1996) 16318–16326.